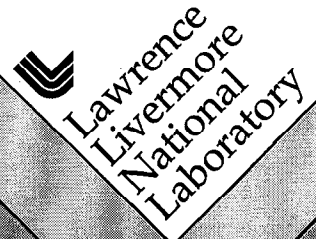# Modeling of Laser Knife-Edge and Pinhole Experiments

C. D. Boley, K. G. Estabrook, J. M. Auerbach, M. D. Feit, A. M. Rubenchik

June 29, 1998

Modeling of laser knife-edge and pinhole experiments

C. D. Boley, K. G. Estabrook, J. M. Auerbach, M. D. Feit, and A. M. Rubenchik

University of California
Lawrence Livermore National Laboratory
Livermore, CA 94550 USA

ABSTRACT

We describe simulations of experiments involving laser illumination of a metallic knife edge in the Optical Sciences Laboratory (OSL) at LLNL, and pinhole closure in the Beamlet experiment at LLNL. The plasma evolution is modeled via LASNEX. In OSL, the calculated phases of a probe beam are found to exhibit the same behavior as in experiment but to be consistently larger. The motion of a given phase contour tends to decelerate at high intensities. At fixed intensity, the speed decreases with atomic mass. We then calculate the plasmas associated with 4-leaf pinholes on the Beamlet transport spatial filter. We employ a new propagation code to follow a realistic input beam through the entire spatial filter, including the plasmas. The detailed behavior of the output wavefronts is obtained. We show how closure depends on the orientation and material of the pinhole blades. As observed in experiment, a diamond orientation is preferable to a square orientation, and tantalum performs better than stainless steel.

1. INTRODUCTION

Spatial filters have been extensively employed in smoothing high spatial-frequency structure in the wavefronts of large laser systems and in providing lens pairs for image relaying[1]. Plasma formation within the pinhole, however, can distort the beam, effectively resulting in pinhole closure[2]. Hence it is of interest to model the plasmas produced by illumination of material edges by intense laser radiation, and to investigate the resulting aberrations in the beam. In this paper, our ultimate goal is to understand the performance of pinholes consisting of four blades, offset from one another along the beamline, with the inner edges defining a square (4-leaf pinholes)[3]. This geometry can reduce or eliminate the mutual interaction of the four plasmas, preventing plasma stagnation on the beam axis. The problem first involves the ability to calculate the plasma produced by a single blade. We do this by modeling experiments[4] in the Optical Sciences Laboratory at LLNL. We then apply these techniques, along with a full propagation code, to model 4-leaf pinholes on Beamlet.

In all cases, the ablated plasmas are calculated via the two-dimensional radiation hydrodynamics code LASNEX[5], developed to model ICF experiments. While we believe this to be the best available code for our purposes, our application of it represents a low-energy extrapolation. Our electron temperatures (of order 50 eV) and edge intensities (about 100 GW/cm^2) are lower than those typical of ICF.

In OSL, following the plasma calculations, the phase profile of a probe beam is calculated via the code HOLOX[6]. The calculational and experimental phase profiles are qualitatively similar in all cases. The calculated phase profile, however, nearly always exceeds the measured phase. It is interesting that the phase contours tend to decelerate at high intensities. At a given intensity, the speeds decrease with atomic mass, although the calculated dependence is somewhat slower than that seen in experiment. In both calculation and experiment, the phases satisfy simple fits in distance and time.

In the pinhole modeling, plasmas are similarly calculated for the blades, and a beam is propagated through the entire spatial filter, including the plasmas. Both the plasmas and the propagation depend on the orientation (horizontal/vertical versus 45°) of the device. The latter orientation allows more room for the diffractive lobes of the beam at focus, and is thus expected, and found, to be preferable. We obtain the output wavefronts for pinholes made of tantalum and of stainless steel. We show that the calculated behavior is consistent with experiment.

2. SIMULATION OF KNIFE-EDGE EXPERIMENTS

The schematic geometry of the OSL experiments[4] is shown in Figure 1. As illustrated there, a pulse of wavelength 1053 nm illuminated a thin blade from the side. We consider blades of stainless steel (treated as iron) and tantalum, which are representative of pinhole experiments. For iron, the pulse duration was approximately 5 ns and the peak intensities ranged from about 40 to 515 GW/cm^2. For tantalum, the pulse was lengthened to 20 ns and peak intensities ranged from 70 to 295 GW/cm^2. The spatial profile of the beam, depicted in Figure 1, was moderately flat over a diameter of 1 mm. The pulses were fairly uniform in time. A probe beam grazed the knife edge at a small angle to the main beam, and streaked interferometry yielded fringes as functions of distance above the blade and time. The diagnostic beam had a width of about 2 mm, which is larger than typical plasmas during the pulse duration. For Fe, the beam was aimed to graze the front edge from below, at an angle of 5°. For Ta, it grazed the rear edge from above, at the same angle.

Because LASNEX assumes cylindrical geometry, the blade was taken to be rotated through a circle of large radius and the beam was extended into an annular shape. The power of the entire annular beam was adjusted so that the intensity on the knife edge remained correct.

When the laser pulse is applied, material is rapidly vaporized. The configuration for Ta at 10 ns, for a beam with maximum intensity of 174 GW/cm^2, is shown in Fig. 2. The outermost zones near the edge have expanded to a width of a fraction of a millimeter, representing a growth of five orders of magnitude. Above the blade, the electron density (Figure 3) tends to decrease exponentially with distance, with the critical density located a few tens of microns from the surface and the density in the outer zones near 10^{18} cm^{-3}. The expansion is approximately circular near the tip. The peak electron temperature, located just in front of the tip, is 43 eV. The peak charge state of about 19 is also encountered here. These quantities increase slowly throughout the pulse. Results for Fe at 139 GW/cm^2 are similar, except that the plasma is larger because of the lower atomic mass.

From the electron density distribution, we calculated the phases of the probe beam by utilizing HOLOX. The phase is given by the integral along a ray:

$$\delta = \frac{2\pi}{\lambda} \int \left[1 - \left(1 - n_e(s) / n_c \right)^{1/2} \right] ds,$$

with $n_c = 10^{21}$ cm^{-3} the critical electron density. Sample probe rays through the Ta configuration are shown in Figure 4. Note that rays aimed to pass within 100 microns of the top of the blade are greatly deflected. We are primarily interested, however, in rays near the top of the plasma, where the electron density is far below critical. These rays accumulate a small phase, proportional to the line integral of the electron density.

The first plot in Figure 5 shows the phase shifts in Ta as functions of distance above the blade, perpendicular to the probe beam path, for several times. The calculated phases decrease nearly exponentially with distance. Experimentally, the phases become difficult to disentangle above $\delta/2\pi = 3$ or below $\delta/2\pi = 0.1$, so they have been somewhat arbitrarily truncated to this range. Note that the experimental phases also tend to decrease exponentially. Although calculation and experiment are not too different at 5 ns, thereafter the calculated phase systematically rises above experiment, reaching a maximum discrepancy of about a factor of 5. As shown in the second plot of Figure 5, the calculated phase shifts in Fe at 516 GW/cm^2 are considerably closer to experiment, differing by a maximum factor of approximately 1.5.

Taking horizontal slices through the plots at a given phase, say the single-wave contour at $\delta/2\pi = 1$, we can calculate the speed of that contour as a function of time. For times greater than a threshold time of a nanosecond or so, this speed turns out to be almost constant in time, both in calculation and in experiment. The calculated speeds for Ta and Fe are displayed in Figure 6. In Ta, the calculated speed increases from 0.4x10^7 to 0.6x10^7 cm/s and exceeds the experimental values by about a factor of two. The linear part of the curve extrapolates incorrectly at low intensity, but we do not consider this significant since LASNEX is not intended to model this regime. In Fe, the calculated speed increases from 0.5 x10^7 to 2x10^7 cm/s. The experimental speeds exhibit the same trend as the calculations, except that the speed is lower by a constant

linear part of the curve extrapolates incorrectly at low intensity, but we do not consider this significant since LASNEX is not intended to model this regime. In Fe, the calculated speed increases from 0.5×10^7 to 2×10^7 cm/s. The experimental speeds exhibit the same trend as the calculations, except that the speed is lower by a constant offset. The calculated points lie far above the error bars at the lowest intensity, but nearly intercept the experimental bounds at the highest intensity. Note that the speeds appear to level off with intensity.

In experiment[4,7], the 2π phase speed for metals (Al, Fe, Mo, and Ta) is found to vary with atomic weight as $A^{-1/2}$, as shown in Figure 7. This dependence would be expected if the speed were proportional to the ion acoustic speed and $<Z>T_e$ were similar for the materials. Our modeling results for Fe, Mo, and Ta vary as $A^{-0.3}$, but the exponent might change if lighter metals were included.

We conjecture that the main reason for disagreement between model and experiment is the two-dimensional restriction of LASNEX. In a three-dimensional expansion, one would expect a lower speed, consistent with experimental indications. In addition, LASNEX does not contain a detailed model of the vaporization process.

Finally, we remark that, for both model and experiment, the movement of the phase contours satisfies a simple fit of the form

$$\delta(x,t)/2\pi = \exp\left(\frac{v_a(t-t_a)-x}{v_b(t-t_b)}\right),$$

where v_a, t_a, v_b, and t_b depend on intensity and material. This fit is valid for times greater than t_a and t_b, typically of order 1 ns, which are a measure of the time required for the electron density to attain its exponential profile. Setting the numerator to zero, we see that v_a is the one-wave speed. Differentiating the relation with respect to x, we see that v_b is related to the speed with which the phase lines become more horizontal, giving a measure of the expansion speed as a whole. It is possible, as we have found, for the 1-wave speeds to agree better than the phases as a whole.

3. SIMULATION OF PINHOLE EXPERIMENTS

We now apply the knife-edge modeling techniques to a 4-leaf pinhole within the Beamlet transport spatial filter, which has a focal length of 900 cm. We are concerned with an angular half-width of 100 µrad, corresponding to a distance of 0.9 mm. The blades are separated by a short distance (2.7 mm) in order to avoid plasma accumulation along the centerline. The width of an individual blade is about 0.25 mm, as in the OSL experiments. In the square orientation, the blades are set horizontally and vertically, while in the diamond orientation the apparatus is rotated by 45^0. One expects the latter orientation to perform better than the former, since the blades are rotated away from the horizontal and vertical lobes of the focal spot. Propagation calculations without a pinhole, for a typical aberrated beam, show that the field is fairly uniform for a few millimeters on each side of the point of best focus. In each orientation, therefore, the four blades are assumed to have identical time-dependent plasmas, with appropriate displacements and rotations. The power density deposited on a blade varies with position on the blade. To account for the nonuniform deposition, we made LASNEX runs at the midpoint and end of the blade, and we logarithmically interpolated the electron density at intermediate points. In our LASNEX calculations, we took the intensity from the measured field at best focus, in the absence of a filter. We then propagated a beam, starting with a PROP92 input field which gives approximately this vacuum field, through the filter. While this scheme should be iterated, the first iteration gives interesting and useful results.

The propagation was performed by a Fourier transform code (PROPN1) written especially for our purposes[8]. It is capable of describing the full transition between near and far fields. It accepts phase

screens and/or transmission masks at specified points along the beam path. To obtain the phase screens, we divided the plasma associated with each blade into a number of vertical slices and took the phase integral horizontally at (x,y) points throughout the slice. With a dozen or so slices, we could satisfy the numerical requirement $|\delta|<<2\pi$. A single transmission mask specified the actual metallic edges.

The intensity was taken from measurements by D. Milam, for a 20 ns pulse of energy 1.5 kJ (Figure 8). The intensity rises nearly exponentially to about 10^6 GW/cm^2 at the center. The edge intensity at 100 μrad vertically is 34 GW/cm^2, while that at 45° drops to 13 GW/cm^2. The difference between these is due to the diffractive lobes. The intensity distribution scales almost linearly with beam energy.

Figure 9 shows an overall view of the calculated electron densities within a 4-leaf Ta pinhole, at 19 ns during a 20 ns flat pulse of energy 1 kJ. This input pulse is used through the rest of the paper. The plasmas flare away from the edges toward the pinhole center. Note that the plasma for the horizontal blade extends appreciably further into the pinhole than that for the diagonal blade. For a typical plasma of longitudinal length 0.1 cm, the optical phase is shifted by 2π at an electron density of 10^{18} cm^{-3}. The plasma generated by the horizontal blade reaches this density almost at the center of the beamline, so we expect a substantial distortion of the beam. For the rotated blade, on the other hand, this density is located about 0.4 mm diagonally from the center. Figure 10 shows a three-dimensional view of the plasmas, confirming that they do not overlap. Note that the plasmas flare both toward the center and, as is seen more clearly for the square orientation, toward the beam. Again it is evident that the plasmas in the square orientation have the greater extent.

Figure 11 shows the calculated wavefront intensities for a square 4-leaf Ta pinhole, at several time slices, along with the input wavefront. The output is calculated at the relay plane, located two focal lengths downstream from the receiving lens. At 10 ns, plasma effects have not yet become important, and the output field is barely distinguishable from that resulting from the same filter without plasmas. The spatial scale of modulations is about 1 cm, consistent with that expected from a 100 μrad square filter. At 13 ns, the plasma has begun to produce visible distortions, which grow in both scale (to about 5 cm) and amplitude (2:1 peak-to-valley ratio) by 16 ns. The general pattern at 19 ns is similar to that at 16 ns, but the peak-to-valley ratio is now 10:1. The progressive deterioration of the beam in this case is also seen in the contrast, defined here as the normalized variance of the intensity within the central 20x20 cm^2 portion of the beam. The input beam has a contrast of 7.3%. After filtering and propagation to the relay plane, the 10 ns slice slightly decreases in contrast to 6.9%. For later time slices, however, the contrast increases to 13%, 25%, and 68% at 13, 16, and 19 ns, respectively (Figure 12). This suggests a closure time of roughly 13 ns. It is encouraging that, in experiment, the pinhole closed at about 10 ns for a pulse of this energy.

When the pinhole is rotated by 45°, the beam is found to propagate with minimal distortion, giving a final contrast of 6.9% (Figure 13). The intensity of the wavefront has features of order 1 cm, as in the square pinhole at 10 ns. The improved performance of this orientation was also seen experimentally. The pinhole was found to remain open at 2 kJ and to show definite closure at 3.2 kJ.

Retaining the diamond orientation but changing materials, we now consider the performance of an iron pinhole. At a given intensity, the plasma produced by Fe has a greater extent than that produced by Ta, as was shown in the OSL experiments. Thus a greater optical distortion is expected. Indeed, the diamond orientation for Fe fails to remain open. As illustrated in Figure 14, it undergoes closure in about the same manner as was seen above for the square Ta pinhole. At 10 ns, as before, there is little plasma disturbance and the spatial scale is about 1 cm. By 13 ns, however, spatial modulations of a few centimeters are visible and the contrast has tripled. At 16 ns, the scale of modulations has increased to about 5 cm and the contrast has reached 21%. At 19 ns the pattern shows pathologies very similar to those of the square Ta pinhole. A dramatic illustration of this deterioration is shown in the lineouts of Figure 15. Note that the peak-to-valley ratio increases from about 1.5 at 10 ns to about 10 at 19 ns. These calculations appear to be consistent with experiment, in which the pinhole was tested at 1.8 kJ and showed definite closure at 17 ns.

4. CONCLUSIONS

In this paper, we first investigated the interaction of a high-intensity laser beam with a material edge, modeling an experiment in OSL. Using LASNEX, we computed plasma conditions at various times. We then computed the phase shift of a probe beam passing through the plasma. We found that the phase profile behaves very much like experiment, in that the profile decreases exponentially with distance from the blade and that the speeds of the phase contours tend to be constant in time. However, the calculated phases consistently exceed the data. The 1-wave speed decreases with atomic weight in a manner which appears to be slower than experiment.

We then turned to an investigation of 4-leaf pinholes on the Beamlet transport spatial filter. We calculated plasmas for the blades, using the measured intensity distribution near focus. Making use of a new propagation code, we calculated the detailed behavior of a pulse propagating through the entire filter. We confirmed that closure occurs less readily for pinholes set up in the diamond, as opposed to the square, orientation. Results for tantalum and iron pinholes were found to show the same quantitative behavior as experiment, with tantalum performing better than iron.

REFERENCES

1. J. T. Hunt, J. A. Glaze, W. W. Simmons, and P. A. Renard, "Suppression of self-focusing through low-pass spatial filtering and relay imaging," Applied Optics 17, 2053-2057 (1978).

2. J. M. Auerbach, N. C. Holmes, J. T. Hunt, and G. J. Linford, "Closure phenomena in pinholes irradiated by Nd laser pulses," Applied Optics 18, 2495-2499 (1979).

3. J. E. Murray, D. Milam, K. G. Estabrook, and C. D. Boley, "Spatial Filter Issues," these proceedings.

4. D. Milam, J. E. Murray, K. G. Estabrook, C. D. Boley, W. D. Sell, N. D. Nielsen, R. K. Kirkwood, B. B. Afeyan, and Y. A. Zakharenkov, "Pinhole Closure Measurements," these proceedings.

5. G. B. Zimmerman and W. L. Kruer, Comments in Plasma Physics and Controlled Fusion 2, 51 (1975).

6. M. K. Prasad, K. G. Estabrook, J. A. Harte, R. S. Craxton, R. A. Bosch, G. E. Busch, and J. S. Kollin, "Holographic Interferograms from Laser Fusion Code Simulations," Phys. Fluids 8, 1569-1575 (1992).

7. R. V. Smirnov, G. G. Bikmatov, I. N. Burdonskii, V. M. Chernyak, A. Yu. Goltsov, V. N. Kondrashov, N. G. Kovalskii, V. N. Kuznetsov, J. E. Murray, M. I. Pergament, V. I. Petryakov, V. I. Sokolov, E. V. Zhuzhukalo, A. V. Fedorov, and S. N. Koptyaev, "Pinhole Closure in Spatial Filters of Large-Scale ICF Facilities," these proceedings.

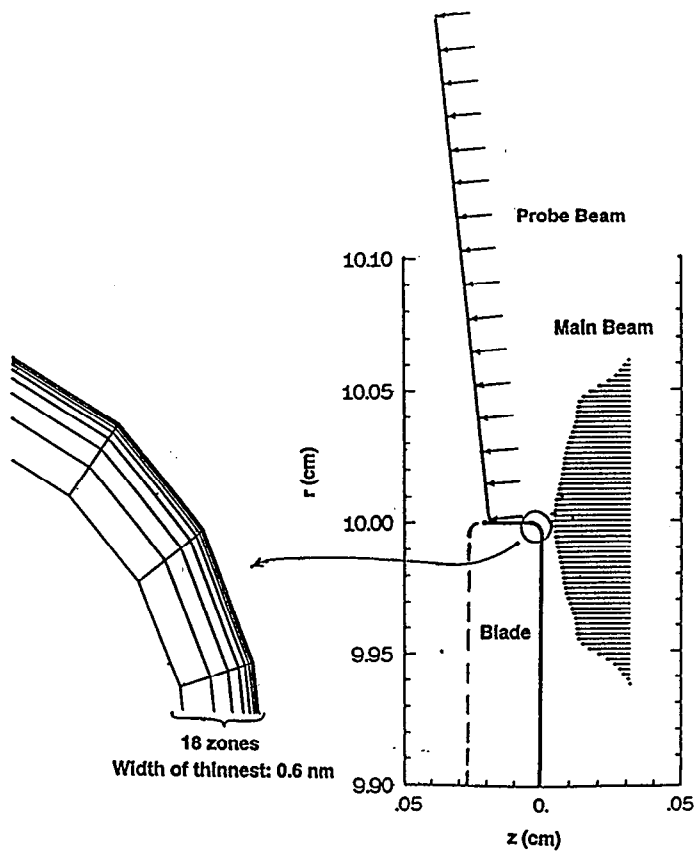8. J. M. Auerbach, PROPN1, Lawrence Livermore National Laboratory (1998).

Figure 1. Schematic geometry of the OSL knife-edge experiment. Zoning of the blade is also shown. Dimensions are in cm. Here and in the next two figures, the top of the blade has been set at 10 cm.
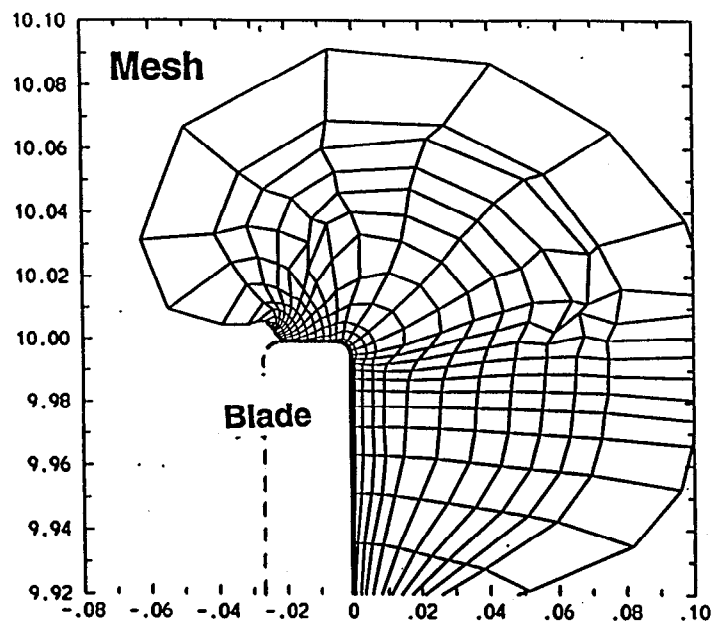

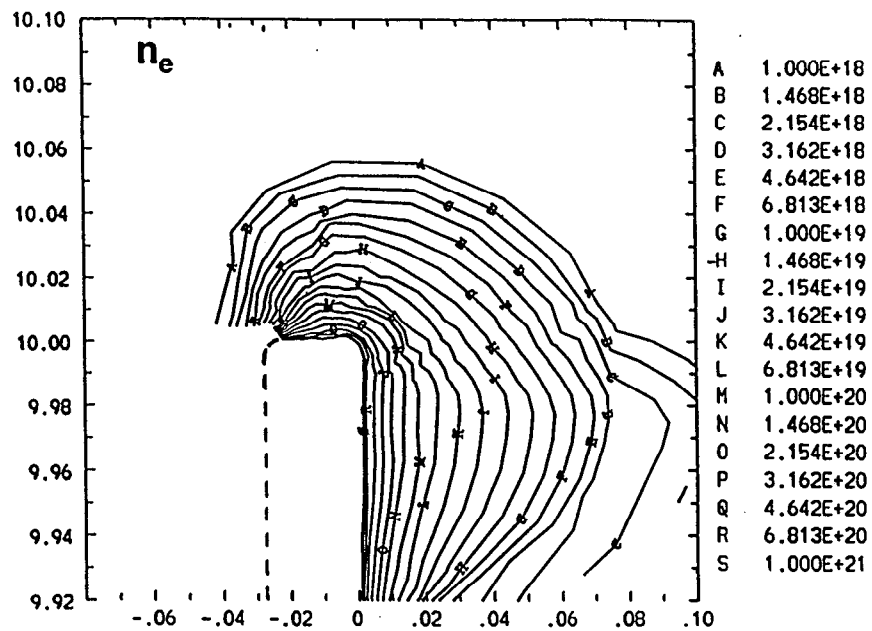Figure 2. Zones at 10 ns, for the OSL beam at 174 GW/cm^2, illuminating a Ta blade.

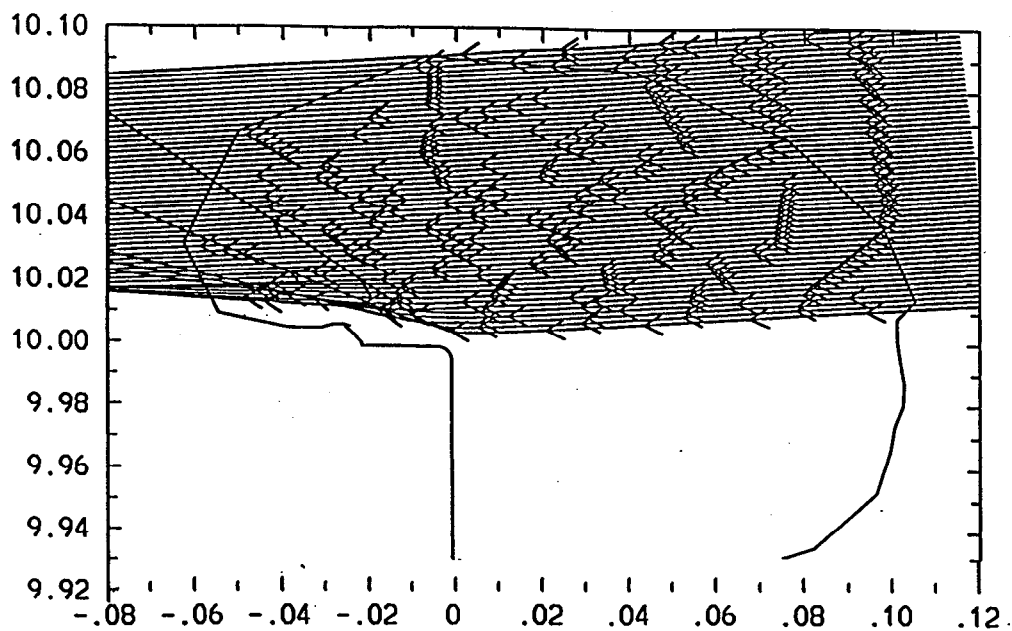Figure 3. Electron density (cm⁻³) in the previous case. Note that the contours differ by a constant multiple.

Figure 4. Probe rays through the plasma, for the last case. Rays scattered beyond a particular maximum angle are not shown.
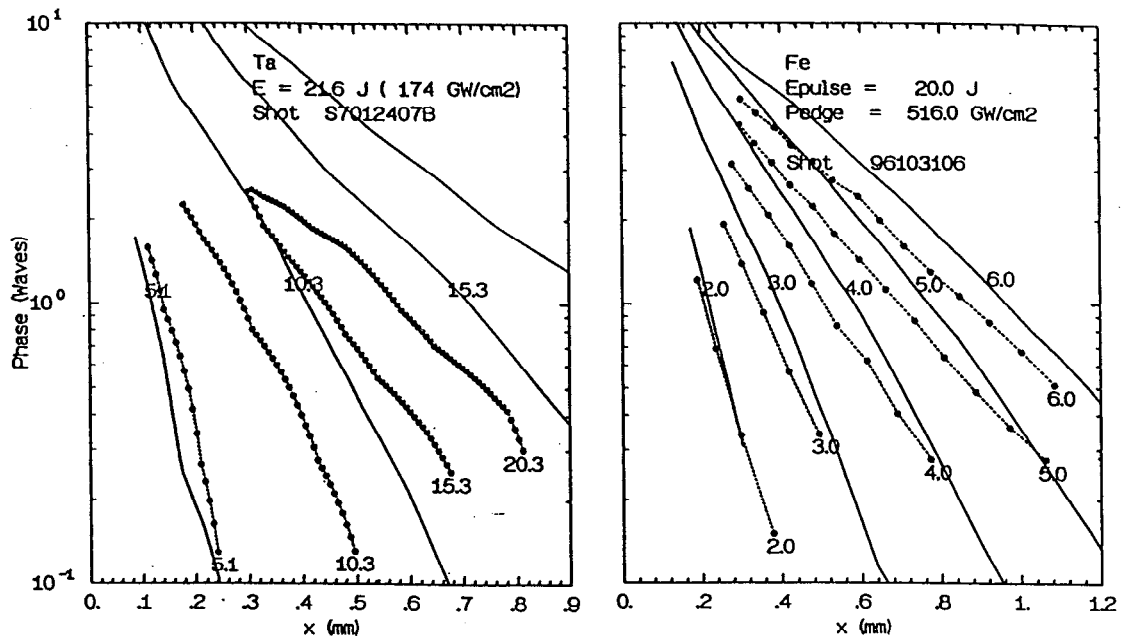
Figure 5. Calculated (lines) and measured (dots) phase shifts versus distance at selected times, for illumination of Ta at 174 GW/cm^2 and Fe at 516 GW/cm^2. The numbers indicate times in ns.
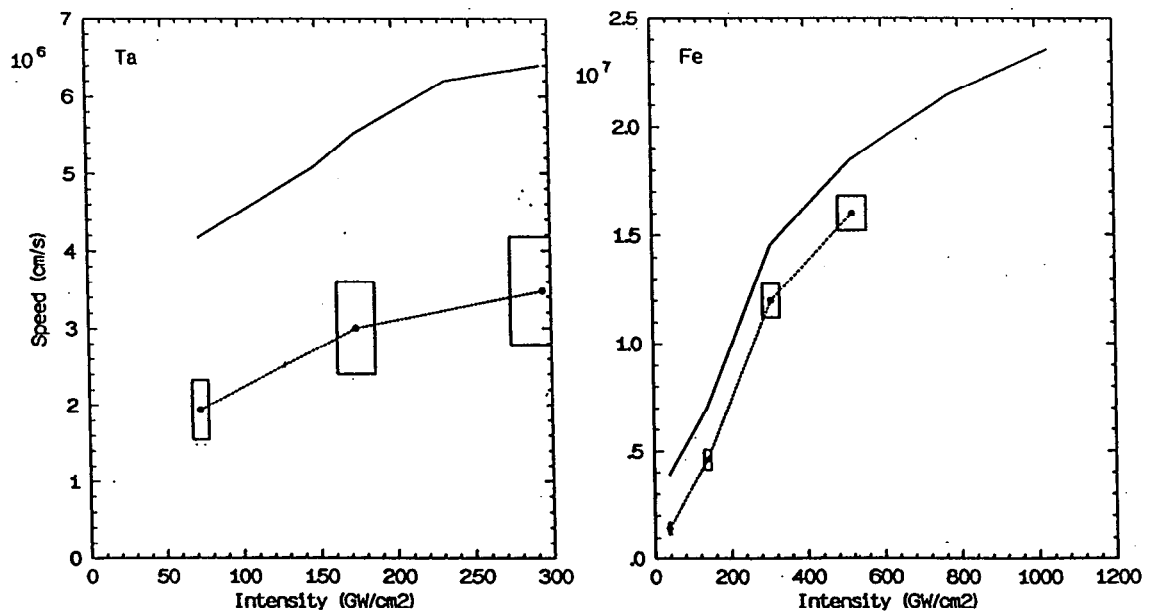
Figure 6. Speed of the 1-wave contour for blades of Ta and Fe, as a function of edge intensity. The rectangles indicate measurements.
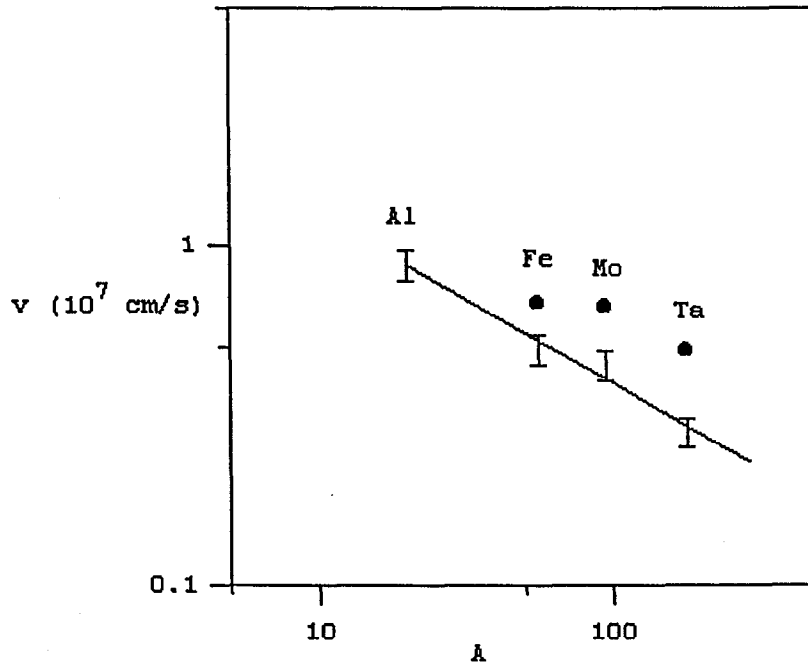
Figure 7. Speed of the 1-wave contour versus atomic weight, for an edge intensity of about 130 GW/cm^2. The slanted line shows a least-squares fit to the data, giving a dependence of $A^{-1/2}$. Calculated points are shown as large dots.
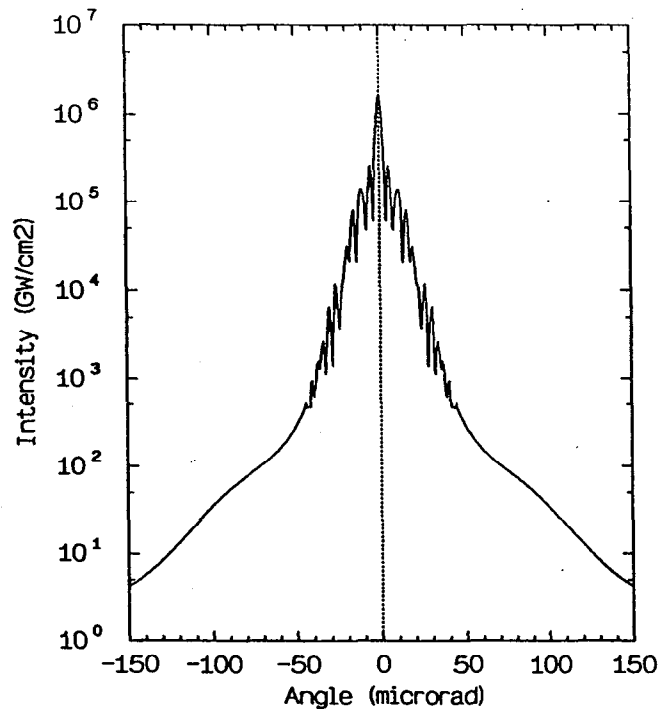
Figure 8. Vertical lineout of intensity at the point of best focus, without a pinhole, for a flat 20 ns pulse of 1.5 kJ (measured by D. Milam). The outer regions have been smoothed.
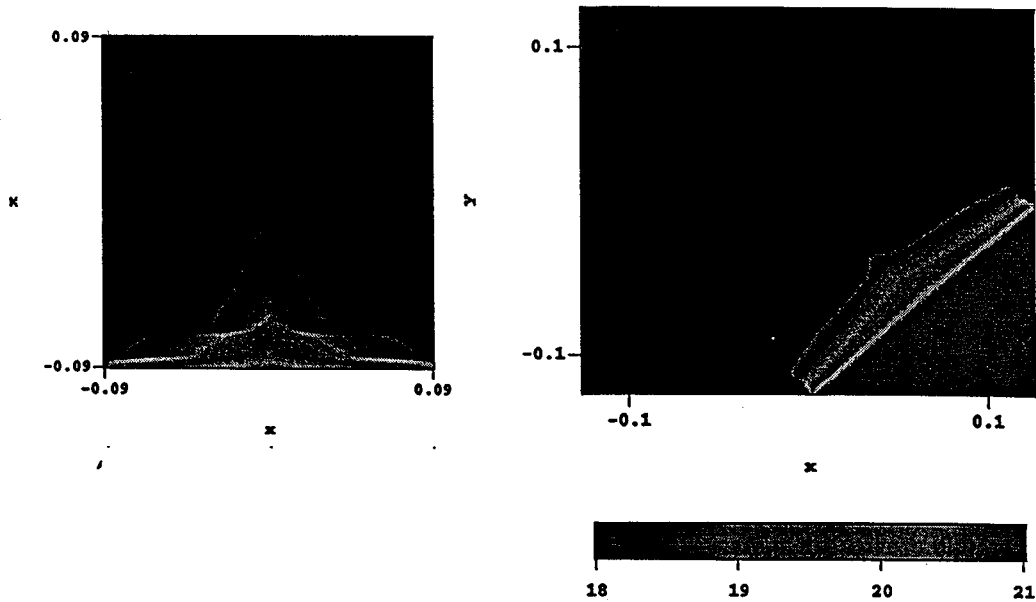
Figure 9. Calculated electron densities along the blades of square (left) and diamond (right) 100 μrad Ta pinholes, at 19 ns during a 20 ns pulse of 1 kJ. The view is along the beamline, at the leading edge of the blade. The color scale gives $\log_{10}[n_e \, (cm^{-3})]$.
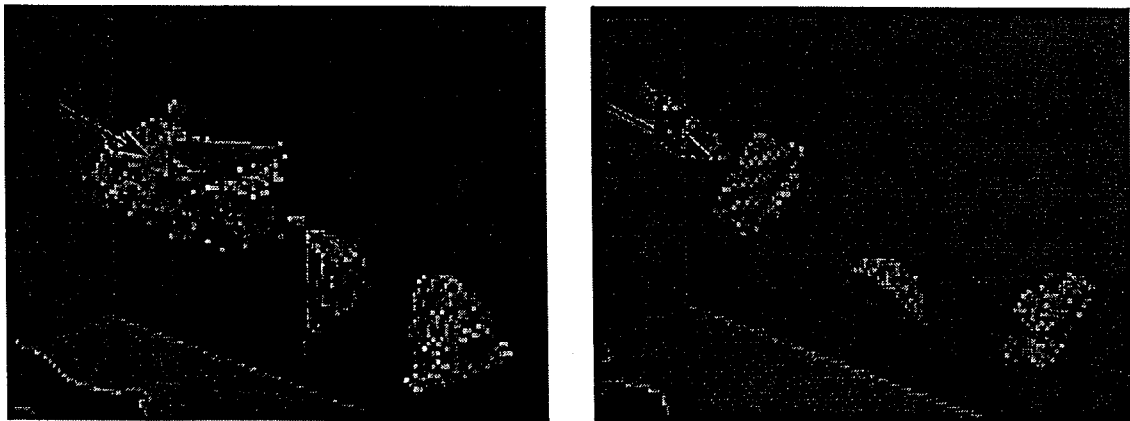

Figure 10. Electron densities as set up for the blades of square and diamond pinholes, as in the last case. Densities greater than 10^{17} cm^{-3} are filled in. The arrows indicate the beam direction.
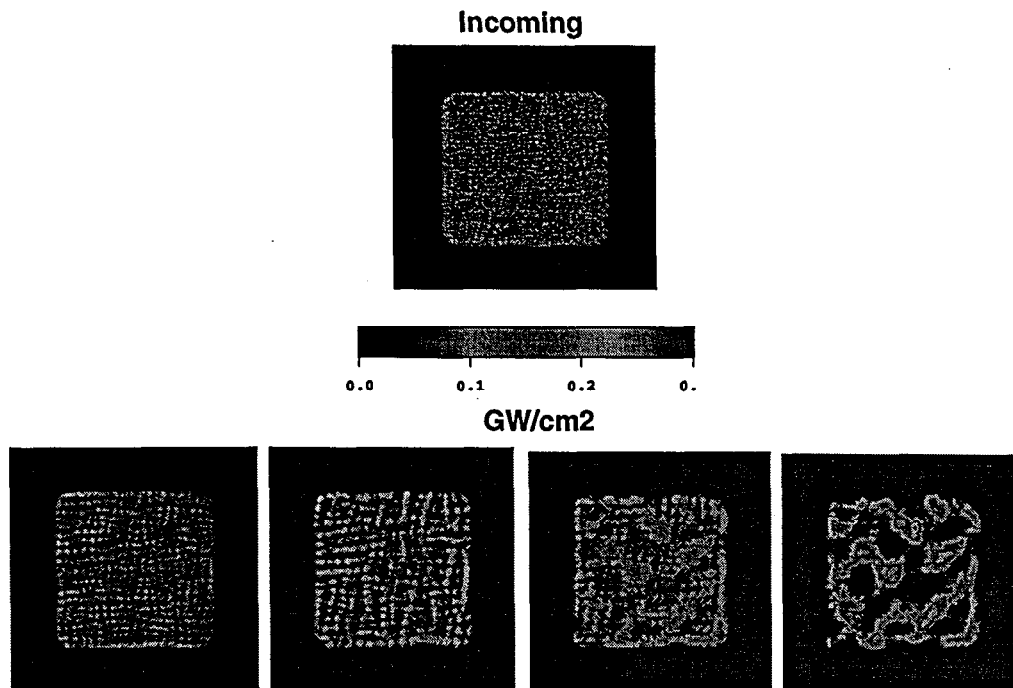
Incoming

GW/cm2

Figure 11. Top: intensity of incoming wavefront for the Beamlet calculations. Bottom: output wavefronts at the relay plane, for a square 100 μrad Ta pinhole, at time slices of 10, 13, 16, and 19 ns.

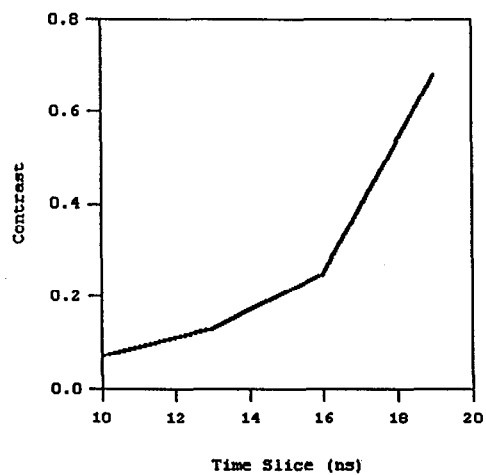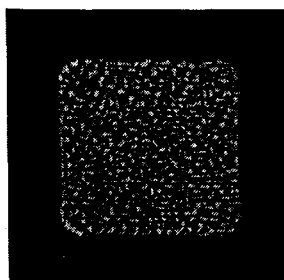
Figure 12. Contrasts of time slices in the last case.

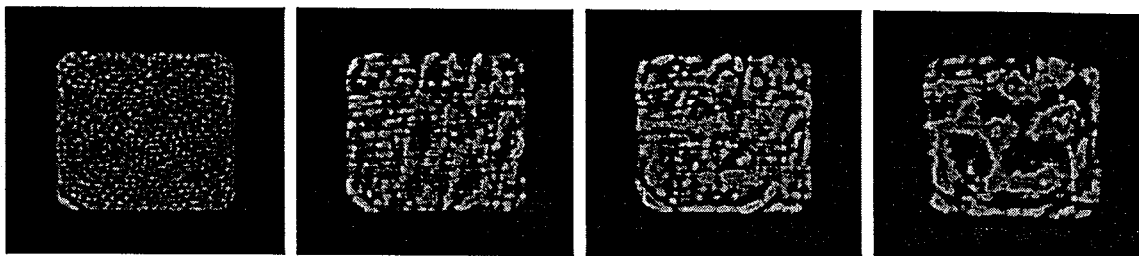Figure 13. Output wavefront as calculated at 19 ns, for a diamond 100 μrad Ta pinhole.

Figure 14. Intensity distribution of output wavefront at the relay plane for time slices of 10, 13, 16, and 19 ns, for a diamond 100 μrad Fe pinhole.
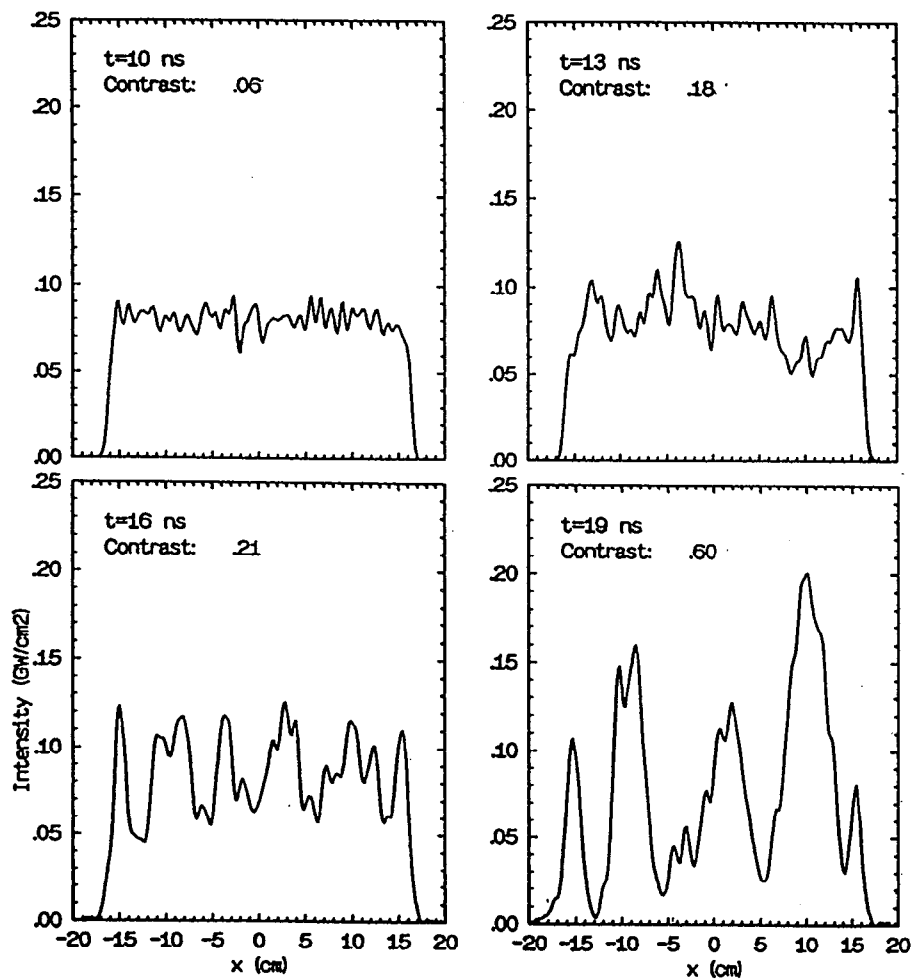

Figure 15. Calculated lineouts through x (at y=0) for the last case.